1 **Ice buttressing-controlled rock slope failure on a cirque headwall,**

2 **English Lake District**

3

4 Paul A. Carling[a, b,] John D. Jansen[c], Teng Su[d, e], Jane Lund Andersen[f], Mads Faurschou

5 Knudsen[f]

6 [a] Geography and Environmental Science, University of Southampton, Southampton, SO17

7 1BJ, UK.

8 [b] Lancaster Environment Centre, Lancaster University, Bailrigg, Lancaster, LA1 4YW, UK.

9 [c] GFÚ Institute of Geophysics, Czech Academy of Sciences, Prague, Czechia.

10 [d] University of Chinese Academy of Sciences, Beijing 100049, China.

11 [e] Laboratory of Water Cycle and Related Land Surface Processes, Institute of Geographical

12 Sciences and Natural Resources Research, Chinese Academy of Sciences, Beijing, 100101,

13 China.

14 [f] Department of Geoscience, Aarhus University, Aarhus, Denmark.

15

16 Corresponding author: Paul A. Carling (p.a.carling@soton.ac.uk)

17

18 **Key Points**

19 Geometry and mechanics of cirque rock slope failure defined from the local geology

20 Rock slope failed slowly due to ice buttressing the cirque headwall

21 Rock slope failure occurred during deglaciation

22

Abstract

Rock slope failures in the English Lake District have been associated with deglacial processes after the Last Glacial Maximum, but controls and timing of failures remain poorly known. A cirque headwall failure was investigated to determine failure mechanisms and timing. The translated wedge of rock is thin and lies on a steep failure plane, yet the friable strata were not disrupted by downslope movement. Fault lines and a failure surface, defining the wedge, were used as input to a numerical model of rock wedge stability. Various failure scenarios indicated that the slope would have failed catastrophically, if not supported by glacial ice in the base of the cirque. The amount of ice required to buttress the slope is insubstantial, indicating likely failure during thinning of the cirque glacier. We propose that, as the ice thinned, the wedge was lowered slowly down the cirque headwall gradually exposing the failure plane. A cosmogenic ^{10}Be surface exposure age of 18.0 ± 1.2 ka from the outer surface of the wedge indicates Late Devensian de-icing of the back wall of the cirque, with a second exposure age from the upper portion of the failure plane yielding 12.0 ± 0.8 ka. The 18.0 ± 1.2 ka date is consistent with a small buttressing ice mass being present in the cirque at the time of regional deglaciation. The exposure age of 12.0 ± 0.8 ka represents a minimum age, as the highly-fractured surface of the failure plane has experienced post-failure mass-wasting. Considering the dates, it appears unlikely that the cirque was re-occupied by a substantial ice mass during the Younger Dryas Stadial.

Key words:

rock slope failure, Pleistocene glacial cirque, cosmogenic exposure dating, deglaciation, Younger Dryas, English Lake District.

1   Introduction

There are at least 70 known or suspected rock slope failures (RSFs) in the Lake District of NW England that have been associated with the Late Devensian glaciation (Marine Isotope Stage 2: Wilson *et al*., 2004; Jarman and Wilson, 2015a). Such RSFs often are termed 'paraglacial' as they "are part of, or influenced by, the transition from glacial conditions to non-glacial conditions" (Ballantyne, 2002; McColl, 2012). However, the relationship between glaciation, deglaciation, and the occurrence of RSFs remains far from resolved. This paper provides a contribution to further understanding of the topic. Although a few highly modified

55 landforms have been identified tentatively as RSFs and related to time periods before the

56 Last Glacial Maximum (LGM; c., 26.5 ka BP to 19 ka BP, Clark et al., 2009) (Jarman and

57 Wilson, 2015b), the majority of Lake District RSFs have been associated with the end of the

58 Dimlington Stadial (see 'Glacial Context') and the final down-wasting of the Late Devensian

59 ice sheet within NW England. At that time, potential RSFs could have been fully supported

60 or partially supported by residual ice masses in topographic lows. Alternatively, some RSFs

61 could have occurred (Wilson, 2005) following the Scottish Readvance (*c*., 19.3 – 18.2 ka;

62 Chiverrell *et al*., 2018) and the Younger Dryas Stadial (12.9 – 11.2 ka; Rasmussen *et al*.,

63 2006). However, only a few disintegrated RSFs have been dated. In contrast, those that

64 represent steep-slope deformation, or arrested slides, are of unknown age (Jarman and

65 Wilson, 2015b). An arrested hillslope failure occurs when the slipped mass is not evacuated

66 from the source area (Jarman, 2005), but is retained on the lower slope of the footwall. The

67 role of glacial ice in buttressing rock slopes, and thereby preventing failure (Whalley *et al*.,

68 1983; Holm *et al*., 2004; Cossart *et al*., 2008; Le Roux *et al*., 2009; Allen *et al*., 2010; Hilger *et*

69 *al*., 2018), is largely speculative (Ballantyne, 2002; Jarman and Wilson, 2015b; Cody *et al*.,

70 2018; Hartmeyer *et al*., 2020) and controversial (McColl *et al*., 2010), as are the mechanics of

71 slope failure in situations where ice-support progressively diminishes (McColl and Davies,

72 2013; Klimeŝ *et al.,* 2021; Cave and Ballantyne, 2016). The latter two generic issues are the

73 primary focus of this paper.

74

75 Glacial erosion can steepen cirque headwalls to the extent that faulted and/or fractured-

76 rock slopes become unstable (Sass, 2005; Moore *et al*., 2009), if not ice-supported. In

77 addition, the way slopes fail can provide insight to whether ice was present during the slope

78 failure. If ice-buttressed failures can be dated, then RSFs provide a source of information on

79 the timing of the final ice retreat. Here, an arrested (*sensu* Jarman, 2005) translational RSF is

80 described, dated, and the likely controls on the failure are defined and modelled. We test

81 the hypothesis that *a steep, faulted, and unstable rock slope has experienced buttressing by*

82 *glacial ice*. Our study area, which has not been previously identified as a RSF site, is within

83 Great Coum (54.3923° N, 2.6057° W), a small cirque within the southern Shap Fells to the

84 west of the Lune gorge (Fig. 1). A neighbouring cirque is named Little Coum. The Lune gorge

85 (south of Tebay; Fig. 2) separates the southerly extension of the Shap Fells to the west from

86 the Howgill Fells to the east. The site details and glacial context are described below.

87

88

89 Fig. 1: Oblique aerial view, looking southwestward, into Great Coum (Google Earth image).
90 The RSF is arrowed. The green grassy tread of the RSF (just above the arrow) is in sunlight
91 below the cliffed headwall (in shadow). The breadth of the RSF is between 125m and 180m.
92 Little Coum is just out of view to the right. Base image © Google Earth 2014. Scale bar
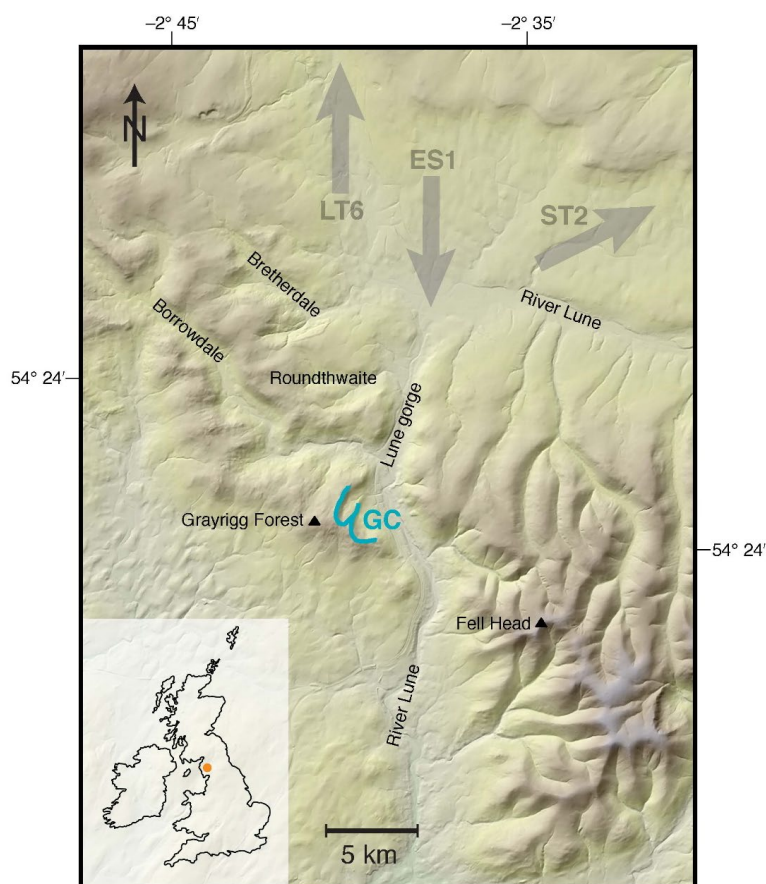93 applies to the middle distance.
94

Figure 2: Regional map showing the location of Great Coum (GC) and Little Coum with respect to generalized Dimlington (e.g., ES1) and (LT6) ice movements (after Livingstone et al., 2010; 2012). Locations referred to in the main text are also shown. Inset shows the location of the study area in the context of the British Isles. Base NEXTMap digital elevation topography has a 5 m resolution.

2   Glacial Context

The last period of extensive glaciation in northern Britain occurred during the Dimlington Stadial of the Late Devensian substage of the Pleistocene (~28-15 ka; Rose, 1985; Scourse *et al*., 2009; Chiverrell and Thomas, 2010; Davies *et al*., 2019), equivalent to Stadials 3 and 2 of the North Greenland Ice Core Project (NGRIP) chronology (Lowe *et al*., 2008) and the Marine Isotope Stage 2 (Ehlers and Gibbard, 2013). During the LGM, the Lune gorge and surrounds were covered by several hundred metres of ice. The Lune gorge is ice-sculpted, having a

110   parabolic bedrock cross-section with truncated valley-side spurs along both the west and the

111   east margins. Great Coum and Little Coum, on the western side of the gorge, are the only

112   recognized cirques in the Lune gorge. These two Lunedale cirques should not be confused

113   with two cirques with the same names in Dentdale (Barr *et al.*, 2017). The two conjoined

114   embayments were considered by Marr and Fearnsides (1909) to be a single cirque, but

115   recently have been recorded as separate cirques (Barr *et al.*, 2017; Clark *et al.*, 2018).

116   Devensian till banks and moraine (entrenched by the River Lune) fill much of the Lune gorge

117   floor and till also occurs in most tributary valleys (Aveline *et al.*, 1888; Marr and Fearnsides,

118   1909; BGS, undated; 2008 a and b).

119

120   **2.1   Complexity of Devensian glaciation around Great Coum**

121

122   The context in which the RSF occurred is relevant to the interpretation of the importance of

123   potential ice buttressing and is referred to within the Discussion. Here we provide the

124   setting. Little is known of the glacial history of the Lune gorge area (Carling *et al.*, 2023).

125   Nevertheless, prior findings, in the main, have been incorporated in the BRITICE maps of the

126   area (Stokes *et al.*, 2018). A complex interplay occurred in the vicinity of the Lune gorge

127   between several upland ice dispersal centres, primarily: the Scottish, Lake District and

128   Howgill ice masses, during the period of maximum ice cover ~ 26–22 ka. All three ice masses

129   interacted in the north whilst the latter two ice masses dominated to the south. After the

130   LGM, as the ice sheets down-wasted and ice flows became increasingly valley-confined, ice

131   emanating from the two cirques would have flowed northwards (Carling *et al.*, 2023).

132

133   The complexity of regional ice flow was simplified by Livingstone *et al*. (2010; 2012) by using

134   codes to refer to different ice streams (Fig. 2) that occurred in various locations and at

135   differing times; the relevant codes are as follows. In the ES1 phase, early LGM, northern ice

136   penetrated a short distance into the Lune gorge (Harkness, 1870; Goodchild, 1875; 1889;

137   Marr and Fearnside, 1909; Hollingworth, 1931; Moulson, 1966; Letzer, 1978) as far as

138   Carlingill and Great Coum (Fig. 2) but no further. However, Davies *et al*. (2019)

139   demonstrated that, close to the LGM, (ST2 phase; *sensu* Livingstone *et al*., 2010) and during

140   the LT6 phase (Chiverrell *et al.*, 2018), ice flowed northwards from the Lune gorge (Fig. 2).

141   On the northern flank of the Howgill Fells, any ST2/LT6 ice flow would have been to the

Earth **Surface**
Dynamics
Discussions

EGU

142   north and east from the Howgill ice dome (Fig. 2) such that the higher summits of the

143   Howgill Fells were not overrun by ice from further north (Gunson, 1966; Stone *et al*., 2010).

144   Rather, the Howgill Fells hosted its own local ice dispersal centre. Prior work failed to

145   determine whether northern ice entered the two Lunedale cirques. Consistent northerly

146   down-wasting ice-flow was established (Hollinsworth, 1931; Rose and Letzer, 1977) from 19

147   ka (Davies *et al*., 2019) with surrounding areas north and south of the Lune gorge being ice

148   free by ~ 19.2 to 16.6 ka (see Carling *et al*., 2023, for a review of regional dates). These dates

149   are broadly consistent with other dates for deglaciation of the central Lake District more

150   widely (Wilson and Lord, 2014) and are indicative of a general ~ 2–3 kyr window for the

151   timing of final Dimlington ice down-wasting within the Lune gorge when the back wall of the

152   Great Coum cirque could have become ice-free. We return to this point in sections 3 and

153   6.2.

154

155   Given that ice may have reoccupied upland terrain in Lake District during the Younger Dryas

156   (Brown *et al*., 2013; Bickerdike *et al*., 2018), in principle, an ice mass may also have occurred

157   in the general vicinity of the Lunedale cirques at this time. However, no evidence for

158   Younger Dryas ice in the Lune gorge has been reported.

159

160   **3   Geological Setting of the cirques**

161

162   The bedrock in the cirques comprises the marine Silurian Coniston Group (Soper, 1999;

163   Soper, 2006), which here consists of fine-grained, blue-grey, sandy siltstone (greywacke) in

164   beds from < 1 m to ~ 3 m thick. Most of the thicker beds crop-out within the headwalls of

165   the cirques. The thicker sandstone beds are more competent with fewer fractures, whilst

166   thinner fissile siltstone beds exhibit cleavage and are heavily fractured. Vertical joints are

167   frequent with spacings of a few metres, together with evidence of small-scale bedding

168   deformation and small-scale faulting. Moseley (1968; 1972) considered the considerable

169   complexity of the regional structure and noted folding, steep discontinuous local faulting,

170   joint patterns and the presence of slickenside surfaces in the southern Shap Fells. In the

171   Methods and the Results, this complexity is not considered, as the detail is not pertinent to

172   our study. None-the-less, reference is made to local steep faults, slickenside surfaces and

173   friability where these are relevant, as the rock structure in the vicinity of the RSF is critical in

174   assessment of slope stability (Bonilla-Sierra *et al*., 2015; Stead and Wolter, 2015). The

175   apparent dips of the local beds range from 0° to 30°, SW into the headwall of Great Coum.

176   However, the apparent 8° plunge of the stratal sequence is towards the NW, such that the

177   true dip is to the WSW with a NW strike (BGS, 2008 a and b). Infrequent, but distinctive 10–

178   40 mm-thick pale bands of siltstone occur (*e.g.,* Taylor *et al*., 1971, p. 26) in some of the

179   thicker beds, which extend discontinuously over distances of several decametres parallel to

180   the primary bedding. These siltstone bands are significant in that examples (here termed

181   marker horizons) occur in the headwall strata which correlate with similar siltstone bands in

182   the strata of the RSF.

183

184   Great Coum is orientated NE, Little Coum is orientated NNE. The orientations of the cirques

185   are influenced by the strike of local paired anticlines (Marr and Fearnside, 1909; BGS,

186   2008a), and the low-insolation aspects of both sites would have encouraged Devensian snow

187   and ice accumulation and preservation. Great Coum exhibits no distinct lip (i.e., no

188   overdeepening), the ground falls steadily from around 237 m (height above mean sea level,

189   m asl) to the River Lune below (Fig. 3A). Above 300 m the ground rises more steeply to

190   rocky head walls locally near 80° at 360–440 m, giving a height range of around 225 m. Little

191   Coum exhibits a slight lip at around 262 m altitude. Above 400 m the ground rises more

192   steeply to near 80° rocky head walls at 400–440 m, and the ridge crest at 480 m gives a

193   height range of around 220 m (Fig. 3B). First to second-order minor streamlets occupy the

194   lower parts of Great Coum, and Little Coum is drained by the third-order stream, Burnes Gill.
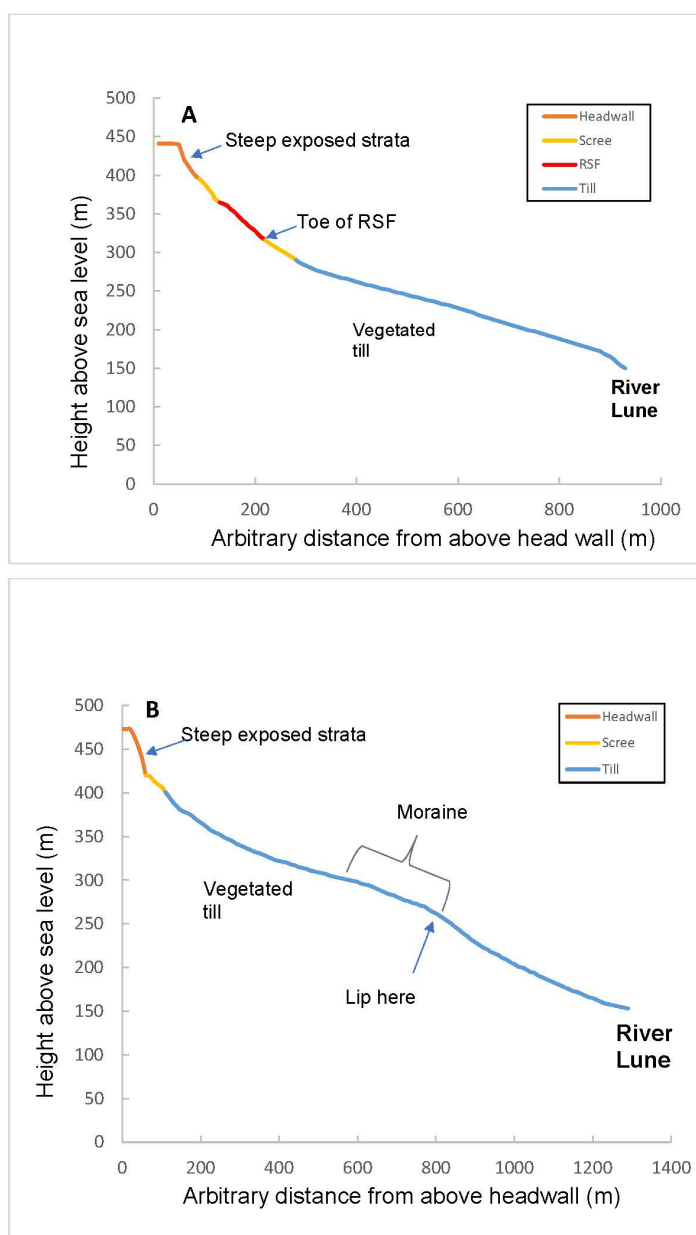
195

196

197

198

199

Figure 3: Long profiles along centre of cirque: (A) Great Coum; transect from 54.389978 N;
2.606625 W to 54.396675 N; 2.598278 W; (B) Little Coum; transect from 54.393789 N;
2.615992 W to 54.400117 N; 2.602208 W. Exposed bedrock is indicated in the headwall and
in the RSF. Data extracted from Google Earth.

204

205   The British Geological Survey (BGS,2008b) map identifies till on the lower slopes of Great

206   Coum and the BGS borehole database contains the records of 24 shallow boreholes ranged

207   along the axis of the Lune gorge over 1.25 km immediately below Great Coum. These

208   borehole logs show that the slopes just below the cirque consist of a thin soil above a 2.5 m

209   thickness of Devensian diamicton, overlying the Silurian Coniston Grit. In Little Coum,

210   hummocky till infills the cirque below 400 m (BGS, 2008b); at lower altitudes, a flatter thin

211   diamicton drapes much of the basin, including a poorly defined curvilinear moraine that

212   terminates at the lip (Fig. 3B). It is not possible to calculate an equilibrium line altitude (ELA)

213   with any certainty based on the upper limit to highest lateral limits to the curvilinear

214   moraine (Porter, 2001), but 300 m asl is a reasonable estimate. Bedrock exposures along

215   Burnes Gill and augering during the current project indicate that this moraine is no more

216   than 6 m thick. The curvilinear moraine has a distinctive, sharp, outer margin along the

217   rocky rounded ridge that separates the two cirques. Within Little Coum, three faint

218   diamicton-covered (possibly ice-recessional) benches occur on the northern slope of the

219   cirque. Thus, although Great Coum lacks any preserved indication of ice retreat, such

220   indicators may exist within Little Coum.

221

222   All the deposits described above are significant. In the first instance, substantial till in the

223   Lune gorge below Great Coum has been related to northern ice penetrating the gorge

224   around the LGM (Carling, *et al*., 2023). At that time, the whole region was covered by a thick

225   ice sheet (Merritt *et al*., 2019). However, as down-wasting led to increasing topographic

226   control and valley glaciers predominated, there was likely to be ice flow out of the cirques

227   prior to the near-complete ice retreat that left the diamicton-covered benches. We envisage

228   that around the LGM, thick overriding ice in the vicinity of Great Coum was dictated by

229   regional ice gradients largely independent of the local topography (Carling *et al*., 2023).

230   Post-LGM, ice-discharge from the cirque initially would have remained high but any

231   buttressing effect on the headwall would decline as the ice thinned.

232

233   The RSF occurred in Great Coum. The most southerly backwall section of the cirque consists

234   of a steep rocky headwall facing N, whilst to the west a further steep rocky headwall faces

235   NE; a steep grassy slope occurs between these two outcrops. The RSF caused headwall

236   retreat in the vicinity of the present grassy slope, leaving the intact steep rocky sections of

237   the backwall to either side, but the failure also extends below the north-facing headwall (Fig.

238   1). Indistinct, small RSFs also occur to the east and west, which are not considered further.

239   Little Coum also contains a steep rocky headwall, but with no evidence of slope failures. The

240   mass of the RSF in Great Coum appears to have descended as a translational near-intact

241   block. Although a near-vertical fracture occurs in the right-hand side of the slipped mass

242   (Fig. 4), in other respects the undisturbed strata within the block readily correlate with strata

243   in the headwall above.

244

245   **4   Materials and Methods**

246   **4.1   Mapping landscape features**

247   The British Geological Survey (BGS, 2008a) records several lineaments in the vicinity of

248   Great Coum that represent small faults or large block joints. Google Earth satellite images

249   (2004, 2009, 2011 and 2014) were used to visually identify these linear landscape features

250   as well as others of relevance (not recorded by the BGS). Lineaments trace topographic

251   discontinuities, stratigraphic offsets, vegetation differences and slickensides, and these

252   forms were checked in the field. Smaller-scale linear features consist of the silt banding

253   marker beds, and numerous minor joints (the latter not mapped). The various points of

254   interest were recorded as single point data in the field using a hand-held Garmin global

255   positioning system (GPS). The strikes of bedding and the direction of faults were recorded

256   as compass bearings whilst the dips of bedding and faults were recorded relative to a

257   horizontal plane using a digital clinometer.

258

259   Single point data are precise in planview whereas linear features, between two or more

260   well-determined points, provide the general trend of features such as gullies and faults.

261   GPS coordinates also were used to map the extent of the slumped block. Due to the

262   inaccuracy of hand-held GPS-derived altitudes, the planview GPS coordinates were used to

263   determine the altitude of each point from Google Earth, and these were taken as definitive

264   (error < 4%) after cross-checking with Ordnance Survey 1:50,000 maps (Harley, 1975).

265   Selected topographic profiles were also developed from Google Earth imagery by reading x,

266   y and z coordinates at 10m horizontal spacings along selected planview lines running from

267   the top of the headwall of each cirque, across the free face and the slope below. Finally, a

268   systematic search was made within both cirques for Shap granite or limestone erratics to

269   check whether northern ice had entered the cirques. Outcrops of both these lithologies

270   occur 10km to the north.

271
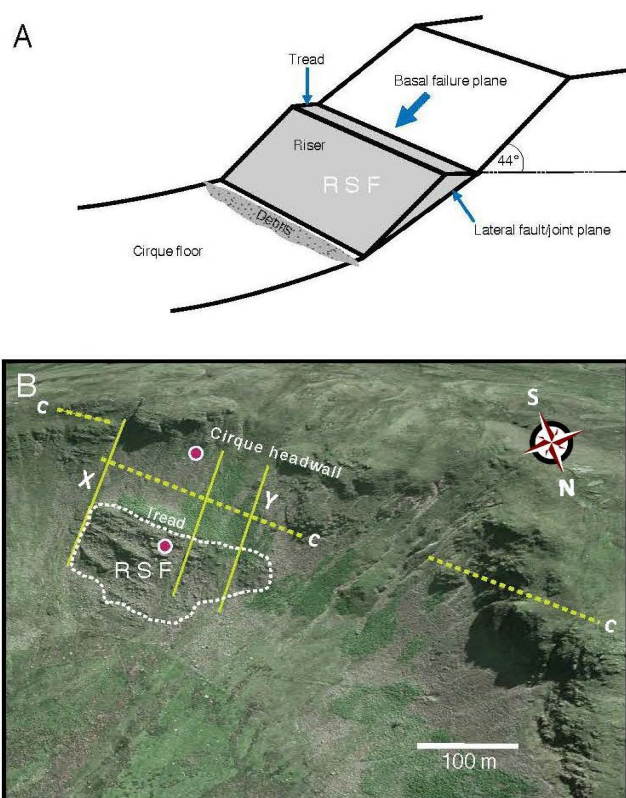
Figure 4: A) Schematic cartoon of a simple wedge failure to indicate the terminology used
within the main text. B) Annotated view of Great Coum (compare Fig. 1). The fault-aligned
rock slope failure plane (c), above and behind the RSF, is intersected by three major steep
fault lines, the outer two of which (X,Y) define the RSF model. The locations of samples (HW
and OSF) collected for exposure dating are shown by circled symbols. Base image © Google
Earth 2014. Scale bar applies to the middle distance.

278

279   We refer the reader to Figure 4A for an explanation of the RSF terminology used here,

280   although the failure planes bounding the wedge are omitted for clarity. The modern

281   headwall of the cirque locally constitutes the main exposed scarp of the failure plane behind

282   the translational wedge of the RSF. The outer face of the wedge is termed the 'riser' and the

283   near-horizontal head of the wedge is termed the 'tread'.

284

4.2   Rock sampling for surface exposure dating

286   Terrestrial cosmogenic radionuclides, such as [10]Be, are produced and accumulate in minerals

287   within a few metres of Earth's surface due to their exposure to secondary cosmic rays and

288   are lost via erosion and radionuclide decay (Lal, 1991). In our case, two free rock surfaces

289   are recognised (Fig. 4): the riser, being the outer surface of the RSF, and the tread, which

290   forms the top surface of the slipped mass. We set out to determine when the RSF riser was

291   first exposed to cosmic rays as ice receded from the cirque. For reasons of economy, we

292   collected one sample from the riser to compare the exposure age with the timing of

293   regional deglaciation. A ~15 kg intact block of bedrock (sample OSF) was collected from the

294   outer 10 cm-thick surface of the riser (Fig. 4B); a prominent thick undisrupted stratum close

295   to the top of the RSF mass. Our sampling strategy was restricted by the ease of access and

296   by the nature of the bedrock surfaces. The smooth bedrock surface of the riser we sampled

297   suggests minimal loss of rock mass due to surface fragmentation or spalling since the RSF

298   occurred. A second 15 kg bedrock block (sample HW) was collected from the failure plane

299   of the transverse fault line just below the cirque headwall (Fig. 4B) with an aim to

300   determine the timing of the failure. The sampled bedrock failure plane was observed to be

301   densely fractured, suggesting some loss of material from the surface since its exposure.

302   Surface erosion affects the abundance of cosmogenic nuclides and the estimated exposure

303   age; an issue we address in the Discussion (and Supplementary Materials). Samples were

304   cut from *in situ* bedrock surfaces using a powered rock saw, and their altitude, bearing, tilt,

305   and topographic shielding were recorded. Topographic shielding is significant for both

306   samples; details are given in Fig. S1 (Supplementary Materials).

307

308   Our approach entails three important assumptions about the last glaciation. First, we

309   assume that the cirque headwall experienced at least 2 m of bedrock glacial erosion, which

310   removed the nuclide inventory produced during preceding ice-free periods; and second, that

311   ice burial depth at the position of the OSF sample was at least 20 m and therefore sufficient

312   to effectively halt nuclide production and third, that this cover persisted until failure. These

313   assumptions mean that sample OSF began accumulating [10]Be only from the time that the

314   down-wasting ice exposed the surface to cosmic rays. In contrast, sample HW remained

315   deeply shielded (> 5 m) within the cirque headwall until the RSF exposed the failure plane

316   to cosmic rays.

317

318   **4.3   Cosmogenic nuclide analysis**

319   The two bedrock samples were prepared for cosmogenic [10]Be analysis at the Aarhus

320   University Cosmogenic Nuclide Laboratory, Aarhus, Denmark, following standard laboratory

321   procedures as described in Andersen *et al*. (2020). The [10]Be/[9]Be ratios were analysed at the

322   accelerator mass spectrometer at AARAMS, Aarhus, Denmark. A summary of the

323   cosmogenic nuclide analyses is given in Table 1 and further details are found within

324   Supplementary Materials.

325

326   **Table 1.** Summary of the cosmogenic nuclide analyses. [10]Be concentrations in quartz
327   normalized to the "07KNSTD" standardization by Nishiizumi *et al*. (2007), and exposure ages
328   calculated using LSDn scaling (Lifton *et al*., 2014) and global calibration dataset (Borchers *et*
329   *al*., 2016) via http://hess.ess.washington.edu v3.0.2. The analytical uncertainty includes AMS
330   error on measured ratios incl. standard uncertainty of 1.1. %, Be carrier concentration, and
331   processing blank propagation (<1.2 %). The total uncertainty also includes production scaling
332   and calibration uncertainties. Rock density was assumed as 2.7 g cm[3].

333

Sample ID	Latitude	Longitude	Elevation	Topo shielding correction	Sample thickness	[10]Be	Uncert	[10]Be age	Analytic uncert	Total uncert
			(m.a.s.l.)		(cm)	(at g^{-1})	(at g^{-1})	(ka)	(kyr)	(kyr)
HW	54.3907	−2.6065	415	0.74	1	57499	1975	12.0	0.4	0.8
OSF	54.3917	−2.6064	348	0.58	1	63969	2017	18.0	0.6	1.2

334

335   **4.4   Rock slope failure modelling**

336   The RSF was modelled using *Swedge* version 6.0 (2018), a specialised rock-slope stability

337   software package, which can analyse a five-sided block (pentahedron) as a translational

338   wedge-failure—whereby a rock mass slides along a persistent basal plane of failure

339   bounded on each side by a fault or joint plane (Hoek and Bray, 1981; Rocscience Inc., 2018).

340   Either, or both, laterally bounding faults can act as additional slide planes, depending on

341   the geometry of the problem (Fig. 4A). In our case, two surfaces are not confined by

342   neighbouring bedrock: the outer surface of the RSF, the riser, and the top surface of the

343   slipped mass, the tread (Fig. 4). As well as varying the geometry of the failure and the

344   roughness of the failure planes, *Swedge* has options to consider the influence of: (i) a

345   tension crack at the back of the failure (not shown in Fig. 4A); (ii) water in the failure planes;

346   and (iii) the effect of any retaining normal stress that may counter the propensity to slide.

347   In engineering applications, restraining normal stress is conventionally realized using steel

348   rock bolts, or stone and concrete structures applied to the face of the riser, especially near

349   the toe. In contrast, here the issue is whether an ice mass in the cirque can buttress a slope

350   that is otherwise unstable, as is explored below. In glaciated mountain environments,

351   permafrost (and ice segregation) can penetrate bedrock to a depth of several metres

352   (Andersen *et al*., 2015). Ice-filled fissures tend to be stable at temperatures below –2°C,

353   which gives rise to the concept of 'ice-cemented' fractures (Ballantyne, 2018).

354   Consequently, the possibility that permafrost stabilized the RSF failure planes is considered

355   in section 5.3.

356

357   *Swedge* was implemented adopting the Mohr-Coulomb failure criterion (*e.g.,* Jaeger and

358   Cook, 1979) pertaining to the limit equilibrium stability of a three-dimensional rock mass

359   using field data (Table 2). Further details are provided in the Supplementary Materials and

360   within the Results. Stability is defined in terms of a factor of safety (*F*) where *F* > 1 indicates

361   a stable slope and *F* < 1, a failed slope. *F* = 1 represents a critical state. In general terms,

362   the factor of safety is defined as the ratio of the forces resisting motion to the driving forces.

363   Driving forces include the mass of the wedge accelerated through gravity and water

364   pressure; the latter applied normal to each wetted plane. Resisting forces arise from the

365   shear strength of the wedge sliding planes. Any ice load on the wedge is considered only as

366   a weight force contribution to the normal stress. Thus, active support due to the load of any

367   glacial ice (or firn) on the riser is included in the analysis as in Equation 1; where T_n is the

368   normal component and T_s is the shear component of the force applied to the riser. Active

369   support is assumed to act in such a manner as to decrease the driving force in the factor of

370   safety calculation:

371

372   $$F = \frac{resisting\ force + T_n\ \tan\phi}{driving\ force - T_s}\qquad(1)$$

373

374   Unless parameter values are known exactly, a single deterministic RSF model cannot be

375   resolved using Equation 1. In view of the uncertainty, in our field case, related to the exact

376   relationship between fault plane alignments and dips, a variety of potential failure

377

Table 2. Parameter values for RSF as determined in the field and as explored within the three model scenarios.

	Riser Angle °	Tread Angle °	Riser length (m)	Riser Bearing °	Width of tread (m)	Breadth of RSF (m)	Failure Plane Dip °	Failure Plane Bearing	Failed volume (m³)	Fault X Dip orientation °N	Fault Y Dip orientation °N	Fault X bearing °N	Fault Y Bearing °N	Fault X Dip °	Fault Y Dip °	Tension crack
Field	53	1	70	24	15	179	44	11	Est: 68288	291	298	21	28	unknown	unknown	unknown
Model 1	53	1	75	24	15	182	44	24	68333	201	208	21	28	80	72	none
Model 2	53	1	75	24	15	182	44	24	67792	90	90	21	28	71	71	none
Model 3	53	1	110	17	15	125	44	11-14	68739	111	62	21	28	90	62	present

378

379   scenarios must be considered. To narrow the number of models, we used preliminary trials

380   of our field-derived parameter values as input, varying both strength and slope and

381   geometry parameters. Then, consideration of a range of fault plane dips allowed us to

382   exclude geometrically impossible configurations and those geometries that did not

383   resemble the geometry of the RSF. In this manner, we devised three model scenarios that

384   represent the RSF in terms of shape and mass. More than 10,000 simulations were

385   performed for each scenario, varying parameter values systematically (typically ± 10%) to

386   isolate the most probable model for each case. The uncertainty and probability analyses

387   were conducted using the dedicated approaches built into the *Swedge* platform, selecting

388   normal distributions to describe the possible range of parameter values; for example, ± 10°

389   of dips measured in the field. Finally, the buttressing effect of any glacial ice against the

390   potential RSF is considered by applying an external load evenly across the area of the riser

391   to counter any propensity for failure.

392

393   **5.0   Results**

394   **5.1   The rock slope failure**

395   The positions of the pale silt marker beds, located in the headwall and within the RSF,

396   indicate the RSF has moved downslope by about 110 m (*H*) vertically and up to 192m (*L*)

397   horizontally. The width of the tread is about 15 m; the breadth of the slide is between 125

398   and 180 m and the vertical extent of the main slipped intact mass along the outer face (the

399   riser) is about 70 m. Assuming the displaced block is a triangular wedge thinning towards

400   the toe (Fig. 4), the volume of the intact slip is ~ 68,250 m^3. Below the main slip there is an

401   area of disintegrated rubble which could increase the length of the riser, potentially adding ~

402   3 % (~ 2300 m^3) to our volume estimate (Table S1 Supplementary Materials). The value of

403   H/L is sometimes considered a mobility ratio, whereby large values of L for relatively small

404   vertical displacement (H) can indicate unimpeded rapid descent and a long runout. Given

405   the volume of the RSF, values of $H/L > 0.6$, as here, indicate no excessive runout (Whittall *et*

406   *al*., 2017; Table S1 Supplementary Materials).

407

408   The slope of the riser of the RSF mass is currently ~ 30°, that is, is similar to the static angle

409   of repose. This angle may suggest slow downslope movement rather than rapid failure,

410   which tends to produce slope angles much less than the angle of repose. In addition, there

411   was no evidence of hard-rock end-point control at the toe of the slumping block to impede

412   its descent although the toe has rotated outwards (Fig. 4A). The slope of the riser today is

413   less than the slope of the failure plane (44°), which suggests a portion of the intact wedge

414   may be lying above debris derived by over-running some of the disintegrated thin toe of the

415   wedge (Fig. 4A). It is significant that the stratigraphic layers within the main RSF wedge

416   remain intact, with no evident down-slope dilation and little deformation or fracture across

417   the face of the slipped mass. The apparent plunge of the strata (8 to 10° towards the north),

418   *i.e.,* across the face of the RSF, indicates that the western margin of the slip may have

419   descended slightly further downslope than the eastern margin, as the headwall strata plunge

420   6° to 8° in the same direction. The outer face (Fig. 4B) of the RSF has undergone no evident

421   modification.

422

423

424   As shown in Figure 4B, a distinct fault (BGS, 2008b), normal to the cliff face occurs to the

425   east of the RSF at location X, with undisturbed stratigraphy in the headwall either side.

426   Slickenside structures occur along the basal failure plane (c) that continues across the cliff to

427   the north-west. The fault X is aligned with the south-eastern margin of the RSF (as seen in

428   Fig. 4B), whilst a further fault is evident as a distinct fissure in the RSF, with another fault to

429   the north-west (Y). The easterly dip of these three faults could not be determined accurately

430   although they are steep, consistent with the findings of Moseley (1968; 1972) for the

431   Coniston group in the region (see section 5.3). The basal failure plane defined the back of

432   the RSF, whilst the lateral limits to the RSF model were defined by the two marginal fault

433   lines (X,Y).

434

435   **5.2   Estimation of original angle of the outer slope of the rock surface before failure**

436   To apply the *Swedge* model it is necessary to know the angle of the outer slope of the rock

437   face before failure. From the geometry of the residual RSF mass, with respect to the

438   observed failure plane (Fig. 4B), the RSF can be considered as a translational, plane failure of

439   a pentahedron wedge. Taking a side view, the geometry is triangular (Fig. 4B), so it is

440   possible to calculate the minimum slope of the outer rock face prior to slope failure by

441   repositioning the failed block further up the failure plane. The angle of the failure plane is

442   taken as equal to that of the minimum angle of the slickenside surfaces, 44°, with a bearing

443   of between 6 and 11°. The riser (outer face) of the RSF is 70 m in length and the tread width

444   is 15 m; both lengths could have been slightly larger before fracturing occurred along the

445   basal failure plane and at the toe of the RSF (Fig. 4A). Given the small degree of uncertainty

446   with regard to the configuration of the slope before failure, the length of the failure plane

447   (necessarily longer than the riser of the RSF) was varied systematically at the same time as

448   varying the length of the riser between the measured length of 70 m and 90 m; the latter

449   value includes the small area of disintegrated toe (Fig. 4A). The tread width also is varied

450   between the measured breadth of 15 m and a 'limit' of 20 m to allow for potential

451   disintegration along the failure plane at the back of the tread. Repositioning the RSF upslope

452   in this manner, the slope of the outer face could have been no lower than 53° and if the

453   angle of the failure plane is increased beyond ~ 54°, the resulting lengths of the failure plane

454   and outer face become incompatible with field observations.

455

456   **5.3   The Swedge model of the rock slope failure without ice buttressing**

457   Initial application of the Swedge Model used the field data shown in Table 2. We did not

458   model the stability of the wedge in its present position because the basal friction properties

459   are unknown; whether the toe of the RSF rests on rubble derived from the failure plane, or a

460   bedrock surface cannot be determined. Given that the present angle of the riser is 30° and

461   the basal failure plane is at an angle of 44° it is assumed that the wedge is now stable (F>>1).

462

463   The slope of the riser utilized is that applicable to the rock mass before failure, as

464   determined in the preceding section. The width of the tread and the lateral extent (breadth)

465   of the failed mass are determined from the field data. The summit of the cirque is fairly flat

466   so an outward slope of 1º below horizontal is used for the tread; the model is not sensitive

467   to this parameter. The angle of the failure plane is the minimum value for the slickensides to

468   the south-east of the RSF (which were not disturbed by the slope failure). The model allows

469   for defining the additional effective roughness angle (r) on the failure planes by applying a

470   'waviness' parameter (w) that was determined from the range of recorded slickenside

471   values, following Miller (1988). Other parameters were defined from the field data. It was

472   noted above that the dip of the two lateral delimiting faults could not be determined in the

473   field. However, as local faults tend to be steep (Moseley, 1968; 1972) the model was

474   implemented with the values shown in Table 2 and then varied systematically as reported

475   below. Given the geometry of the problem only three modelling scenarios are necessary to

476   explore the uncertainty in a controlled setting:

477

478   *Model 1: the RSF slides over the basal plane and against Fault Y*. The model aligns

479   the compass orientation of the basal failure plane with the orientation of the riser

480   outer face, which assumes a simple downslope slide. The orientation of Faults X and

481   Y with respect to north are as determined from field data. The X and Y fault dips are

482   steep and both dip to the west. Dips and riser length were varied slightly to optimize

483   the failed volume of the RSF to match the field estimate. In this manner, the model is

484   not consistent with the eastern side of the slip having progressed less far down the

485   failure surface than the western side. Factor of Safety: 0.83.

486

487   *Model 2: the RSF slides along the basal plane and against Fault X*. The model aligns

488   the bearing of the failure plane with the bearing of the slickensides to the east of the

489   RSF, as these define the bearing of the basal failure plane that differs from the

490   bearing of the riser face by 13º. The bearings of Faults X and Y are as determined

491   from field data. The fault dips are steep and both dip to the east. Dips and riser

492   length were varied slightly to optimize the failed volume of the RSF to match the field

493   estimate. In this manner the model is consistent with the eastern side of the slip

494   having progressed less far down the failure surface than the western side. Factor of

495   Safety: 0.86.

496

497   *Model 3: explores the addition of a tension crack to the back of the RSF*. It is not

498   known if a tension crack developed in the actual rock mass before failure, and the

499   properties of the tension crack are determined by the other model attribute values.

500   Including a tension crack, the western side of the RSF extends further down slope

501   than the eastern side, with the lower edge of the model block having a plunge of ~

502   10°, equal to the plunge of the RSF strata in the field. The bearing of the basal failure

503   plane is varied between 6° and 14°. Fault dips are steep, 90° and 62° to the east.

504   Dips and riser length were varied slightly to optimize the failed volume of the RSF to

505   match the field estimate. Given this scenario the RSF slides over the basal plane and

506   against Fault Y. Factor of Safety: 0.52 to 0.83 depending on basal plane bearing.

507

508   Given that there is unavoidable parameter uncertainty, none of the above models is an exact

509   representation of the RSF, although Model 3 is the closest match (Fig. 5). Yet, it is evident

510   that preserving the dip of the basal plane and solving to retain the mass of the failure, any

511   reasonable combination of data leads to a model of the failed block that resembles that seen

512   in nature and, in each case, the Factor of Safety is less than unity. A sensitivity analysis

513   showed that, for reasonable ranges of parameter values (typically ± 10°; outwith those listed

514   in Table 2), usually the geometry of the potential failure did not match that observed and so

515   could be dismissed. Specifically, in the 10,000 simulations of each model, model parameters

516   could be varied (*e.g.,* by ± 5° in the case of angles), retaining a probability of slope failure of

517   96 %. In most cases the factor of safety was between 0.74 and 0.94. In a very few cases of

518   parameter combinations (4 %), a marginal factor of safety of between 1.07 and 1.22 is

519   achieved. In the latter cases, wetting between 20 and 30 % of the fault planes surface areas,

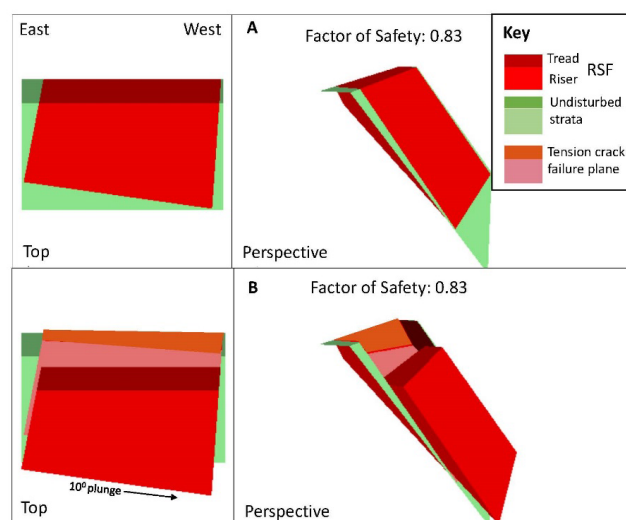520   due to percolation of meltwater, caused the slope to fail.

521

Figure 5: Illustration of Swedge 6.0 Model 3: (A) before failure, and (B) during failure. The basal failure plane orientation is 14º such that the base of the RSF is plunging 10º to the north (right).

As a final consideration it should be noted that in deglaciating mountain regions, RSFs have been related to permafrost degradation and consequent destabilization of ice-filled fractures within the rock mass (Gruber *et al.,* 2004; Gruber and Haeberli, 2007). In the RSF failure model described above, freezing of the failure planes can be considered by simply increasing the friction factors, which can result in the block remaining intact despite the absence of glacial ice buttressing. However, we expect that frozen failure planes did not persist long after glacial down-wasting. Hydrostatic pressure in the failure planes would have high, and percolation more generally lubricates failure planes (Hasler *et al.,* 2011). In addition, permafrost support for the RSF does not explain the intact stratification of the RSF, as permafrost degradation would have resulted in a rapid RSF. Consequently, permafrost was not considered in any quantitative sense.

5.4   The Swedge model of the rock slope failure with ice buttressing

For the range of simulations reported in the previous section, F < 1 in all the 94 % of physically plausible cases and wetting failure planes resulted in a 100 % failure in all 30,000 cases. Hence, the role of ice buttressing of the riser must be considered, as this is the most likely explanation for slope stabilization. There is no information on the dynamic behaviour

544   of ice within the cirque. Consequently, selecting Model 3 above, three contrasting scenarios

545   can be envisaged that might stabilize the slope: (a) ice can be a static load variably

546   distributed around the centroid (Fig. 6A) of the riser; (b) ice can be dynamic, moving towards

547   the riser such that the stress is variably distributed around the centroid of the riser (Fig. 6B);

548   (c) ice can be dynamic, moving away from the riser such that a bergschrund opens between

549   the ice and the slope and the stress is distributed below the centroid of the riser. Broadly

550   consistent results also are found considering Models 1 and 2 (not reported herein).

551

552   Firstly, considering scenario (a), the weight of an ice load is calculated, and the stress is

553   applied evenly across the area of the riser normal (*i.e.,* 90º) to the slope until it is stabilized

554   (for which condition: F = 1.0065; Fig. 6A). Subsequently, considering scenario (ii), the

555   analysis is repeated to ascertain the optimal direction to apply force that minimizes the ice

556   load. In scenario ii, the ice load can be reduced from that in (a) if the force is directed into

557   the slope and slightly upwards by 13^0 above the horizontal such that for F = 1.0485 (Fig. 6B).

558   In scenario (a), application of 40,659 tonnes of ice is required for a stable slope, which is

559   equivalent to 48,987 m^3, based on a debris-free low ice-density of 830 kg m^{-3} (Colgan and

560   Arenson, 2013). In scenario (b), application of 24,325 tonnes of ice (29,307 m^3) is required

561   for a stable slope. For scenario (c), with a tension crack, the slope will remain stable as long

562   as the total stress applied to the slope is the same as for scenarios (a) or (b). In this study we

563   do not explore in detail how the ice mass and force direction might be distributed across the

564   riser to maintain slope stability as there are multiple permutations. Nonetheless, if the

565   cirque had been filled with ice to the top of the riser, around 166,000 m^3 of ice would be

566   required to fill the volume immediately adjacent to the potential RSF (Fig. 7), which is not

567   compatible with the small ice masses in scenarios (a) and (b) that are required to maintain

568   slope stability. Considering Fig. 7, it is important to recognize that, in any permutation of

569   potential RSF geometry (Table 2), the ice cover required to maintain slope stability is

570   typically less than 29 % (and possible as low as 17 %) of the volume to the top of the riser.

571   This result indicates that the slope would have remained stable as long as there was a

572   sufficiently small degree of ice buttressing due to ice in the cirque contributing a stress

573   normal to the face of the riser—which further implies failure occurred during final

574   deglaciation of the cirque. Note that, although the presence of sufficient ice on the riser

575   alone maintains rock mass stability, it is unlikely that this condition would pertain without

576   ice present immediately adjacent to the rock wedge. So, Figure 7 shows cirque ice beyond

577   the unstable slope, but only conceptually.

578

579

580
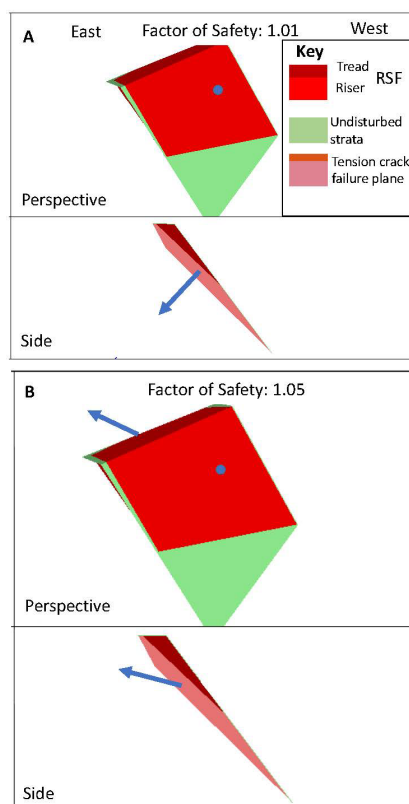
Figure 6: Illustration of the force application required to stabilize the potential RSF: (A) With
the force (point and arrow) applied 90° to the slope, the ice load required to stabilize the
slope (i.e., F = 1.0055) is 40,967 tonnes; (B) With the force (point and arrow) applied at the
optimum angle (13° above horizontal) the ice load required to stabilize the slope (i.e., F =
1.0485) is 28,253 tonnes.
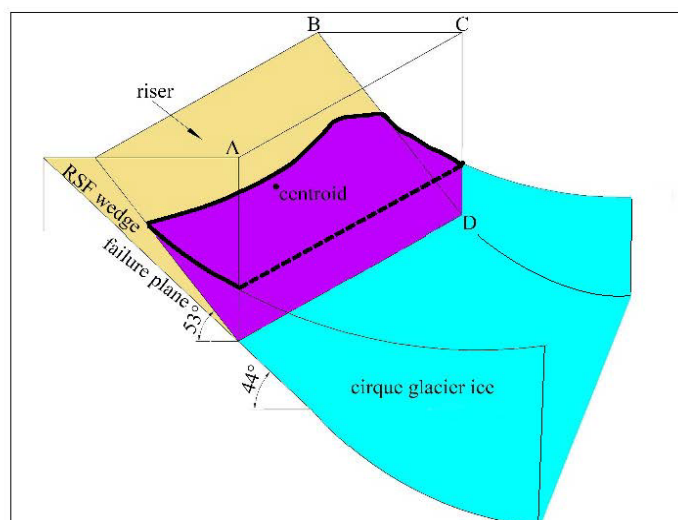
Figure 7: Cartoon depicting the concept of ice buttressing of the potential RSF. The RSF wedge defines the unstable portion of the slope before the rock slope failure. Points A, B, C and D define a pentahedral volume that, if filled by ice, would cover the complete face of the riser. The pentahedral volume, with the upper ice surface outlined by a heavy black line, shows that only a small percentage of the potential pentahedral ice volume is required to be ice-filled to provide buttressing sufficient to prevent slope failure. Percentages were obtained from the ice volumes required to buttress the slope. Additional ice might be present in the cirque outside of the defined volume, but this ice does not contribute to the stabilizing load directly applied to the riser.

5.5   Exposure ages from the rock slope failure

In both cirques, tills are composed of local lithologies exclusively, and a search for northern-derived erratics confirmed their absence. The absence of erratic lithologies indicates that the cirques were probably eroded by locally generated ice masses after the LGM. At the time of the LGM, it is thought that the locations of the cirques were overridden by an ice sheet from the north moving into the northern end of the Lune gorge (Carling *et al*., 2023). Under such thick ice conditions, the back wall of the cirque would have been stable as the volume of ice was much greater than that required for slope stability—shown by either ice-loading Model 3 scenario a or b. During active cirque erosion, after the LGM, the ice volume in the cirque would decrease such that ice-loading also decreased such that the RSF slowly descended as the loading fell below a critical F-value to sustain the slope. It is this lowering of the RSF that we have attempted to date with cosmogenic nuclides.

610   The surface exposure age of 18.0 ± 1.2 ka (sample OSF) postdates the timing of maximum ice

611   cover and is consistent with the timing of deglaciation within the broader region (Carling *et*

612   *al*., 2023) as is considered in the Discussion. As was noted in section 4.2, the outer face of

613   the RSF (the riser) constitutes a smooth surface of intact, undeformed strata, so

614   concordance of the surface exposure age and regional dates is to be expected. Exposure of

615   the RSF riser (sample OSF) predates significantly the exposure age of 12.0 ± 0.8 ka (sample

616   HW) calculated for the RSF basal plane, suggesting a relationship between debuttressing of

617   the riser face and the gradual downward slip of the RSF. The younger age for sample HW is

618   expected, due to the basal failure plane being progressively exposed after the upper portion

619   of the RSF (where sample OSF occurs) was clear of ice cover and the RSF began to move

620   downslope. Also of significance is the fact than the basal failure plane was disrupted by the

621   failure and is friable, as was noted in section 4.2. The loss of only one or two small blocks

622   from the location sampled at any time after failure should result in an age younger than that

623   of the outer face of the RSF (see Supplementary material). Results of the cosmogenic nuclide

624   analyses are summarised in Table 1.

625

626

627   **6.0   Discussion**

628   **6.1 Modelling the RSF dynamics**

629   The *Swedge* model was applied to the RSF assuming the original slope of the rock face was

630   53°, with a slide plane angle of 44° and no ice buttressing. The steeper slickenside surfaces

631   observed in the field directly above the RSF could indicate a steeper failure plane than that

632   used in the model, but these values were not used as they may represent strata disturbed by

633   the RSF. In any case, an increase in the failure plane angle, or the initial angle of the rock

634   face, both increase the propensity for failure. The waviness number calculated from field

635   data and applied in the model is low, which increases the propensity for failure. Preliminary

636   trials showed that to stabilize unstable model slopes would require the use of unrealistically

637   large waviness numbers (Miller, 1988) and so the waviness number was not varied in

638   sensitivity analyses. Thus, our results obtained with the *Swedge* model are conservative but

639   show that the rock face was consistently unstable before failure. The sensitivity analyses

640   accounted for parameter uncertainty and demonstrated that, in most cases, failure would

641   have occurred due to gravity alone. In those few cases where the slope was modelled as

642   marginally stable, moderate water lubrication of the failure surfaces (typically 30% of

643   surfaces) induced slope failure, but the addition of a modest amount of buttressing ice

644   ensured the slope remained stable. As there is no obstacle at the toe of the RSF to impede

645   descent, it is reasonable to assume that the slip occurred slowly as the ice decayed. The

646   need for buttressing of the slope to prevent rapid failure indicates that ice support was

647   important (Hilger *et al.*, 2018). Thus, our hypothesis '*a steep, faulted, and unstable rock*

648   *slope has experienced buttressing by glacial ice*' as proposed in the Introduction is

649   corroborated here.

650

651   As the amount of Model 3 scenario (a) ice (static load normal to the face) in the cirque

652   decreases, the level of the ice against the riser will fall towards the toe. Thus, the focal point

653   of the force applied to the slope by the ice cover migrates down the riser. As long as the

654   stabilizing load and the direction of the applied force remain sufficient as ice retreats, the

655   detached block will remain stable. However, the load within the cirque is unlikely to be

656   maintained as the ice elevation falls. The applied force also is variable through time and

657   across the riser as ice primarily deforms by internal flow (Hutter, 1983) such that, if any

658   additional pressure were exerted by residual ice adjacent within the Lune gorge, then the ice

659   mass within the cirque would respond accordingly. In particular, the uniaxial compressive

660   strength of ice is low and decreases as ice temperature increases, as will be the case during

661   deglaciation. Although in our model we do not consider the shear stresses associated with

662   the ice in a quantitative sense, brittle fracture of the thin, buttressing ice mass might

663   ultimately occur owing to the constant pressure associated with the mass of the RSF (Bovis,

664   1982; McColl and Davies, 2013). The presence of a tension crack will redistribute ice load

665   and induce ice segregation (frost-cracking) in the rock (Sanders *et al.*, 2012) close to the toe

666   of the rock mass, further reducing the competency. So as the factor of safety falls to close to

667   $F = 1$, the detached block will slowly move downwards. In the final stages of deglaciation,

668   low-density firn (~400–830 kg m^{-3}) will replace glacier ice (~830–917 kg m^{-3}) offering less

669   support to the RSF.

670

671   The RSF failure probably was controlled by distinct intersecting small-scale faults, as has

672   been modelled herein. Within the general area of Great Coum there appears to be two sets

673   of frequent lineaments, one trending to N to NW and the other NE, that intersect to define

674   bedrock blocks. Despite this propensity, the other steep headwalls in these two cirques

675   show no evidence of large-scale instability, although the basal fault plane of the RSF extends

676   (Fig. 4) behind the more western steep buttress in Great Coum, indicating that this slope is

677   also potentially unstable. One fault (BGS, 2008b) and several other lineaments occur roughly

678   normal to this alignment which, in conjunction, might delimit a potential wedge failure on

679   this western buttress. In the specific case modelled, slope failure is highly site-specific

680   depending, in the main, on fault alignments. Steepening of the cirque headwall via glacial

681   erosion may have altered the disposition of the rock mass load, increasing tensile stresses

682   along the fault planes, and promoting the RSF (Ballantyne, 2002). In this respect, the failed

683   slope was pre-conditioned (*sensu* McColl and Davies, 2013) to fail. However, the modelling

684   suggests that unloading likely played a role in controlling the timing of failure and the rate of

685   landslide displacement once initiated. Unloading may simply allow the unsupported

686   preconditioned block to fail, but the stress release accompanying unloading usually is

687   propagated along the fault network resulting in a reduction of internal locking stresses (*i.e.*,

688   the waviness number; Wyrwoll, 1977; Ballantyne, 2002). Other preparatory factors also

689   come into play as the ice load was removed, such as lubrication of the failure planes by

690   meltwater and weathering of the fault planes in general, moving the block closer to F = 1.

691

692   **6.2 Timing of the RSF**

693   Although there is only one terrestrial cosmogenic date for the riser of the RSF, the surface

694   exposure dating of 18ka is compatible with the RSF movement during final deglaciation

695   around 19.2 to 16.6 ka (see Carling *et al.*, 2023, for a review of regional dates). We interpret

696   the much younger exposure age (~ 12 ka) on the fault plane as the result of postglacial

697   weathering and erosion. Exposure dating necessarily only yields a minimum-limiting age of

698   exposure, except in cases where primary structures (*e.g.*, glacial striations or slickensides)

699   testify to negligible surface erosion. We observed some slickensides locally preserved on the

700   fault plane, but some degree of surface erosion is also indicated by a scattering of talus and

701   a shattered basal failure plane. We provide an estimate of the magnitude of surface erosion

702   assuming a range of plausible erosion rates in Fig. S2, Supplementary Materials wherein the

703   limitations of having only two cosmogenic samples is addressed.

704

705   We note that the locally derived till and absence of northern derived erratics in the cirques

706   suggests that northern ES1 ice did not enter the cirques, despite the presence of abundant

707   (northern) Shap granite erratics in Borrowdale, Roundthwaite valley and Bretherdale just to

708   the north (Carling *et al.*, 2023). Thus, buttressing of the slope by ice moving into the cirque

709   from the north can be ruled out. We suggest that the two cirques probably fed valley

710   glaciers associated with diminishing plateau icefields after the LGM (Carling *et al.*, 2023), and

711   their final form evolved during deglaciation. The Devensian termination is thought to be a

712   4–5 kyr period of ice decay just prior to the Last Glacial-Interglacial Transition at ~ 14.7–11.5

713   ka (Stone *et al.*, 2010). During deglaciation, there was unlikely to be sufficient ice in the

714   adjacent Lune gorge to bolster the cirque ice mass.

715

716   Regarding slope failures in cirques, Cave and Ballantyne (2016) and Klimeŝ *et al. (*2021)

717   noted that the role of glacial ice support in cirque back wall stability is conditioned by the

718   associated time scales considered. For example, Klimeŝ *et al. (*2021) reported high factors of

719   safety (> 1.95) for potential RSFs beneath glacial ice during the LGM, which is assumed to be

720   the case during full glacial conditions. Ballantyne *et al*. (2014) demonstrated that, following

721   the LGM, the timing of several dated RSFs is not consistent with the probable timing of

722   glacial debuttressing, reporting ages that correspond to deglaciation and well after. In

723   contrast, at Great Coum, the surface exposure age of 18.0 ± 1.2 ka is consistent with regional

724   estimates of the timing of deglaciation (see Carling *et al*., 2023), as was noted above.

725   However, the apparent delay in final exposure of the fault plane, sometime before 12.0 ± 0.8

726   ka, indicates that a range of exposure ages might be associated with arrested RSFs; indeed,

727   some post-glacial dates may be associated with isostatic controls on slope failure (Ballantyne

728   et al., 2014).

729

730   **6.3 An ice advance during the Younger Dryas?**

731   An important remaining issue is whether Great Coum could have supported a glacier during

732   the Younger Dryas Stadial. Although the Lake District was essentially ice-free by ~ 14.7 ka,

733   Younger Dryas cooling led to a subset of cirques in northern Britain refilling briefly (Evans,

734   1997). Sissons (1980) argued that many central Lake District cirques were re-occupied by ice

735   during the Younger Dryas, and subsequent studies (reviewed by Brown *et al*., 2011) indicate

736   the presence of cirque glaciers in the central Lake District. However, the lowest Lake District

737   cirque floors are around 320 m asl (Temple, 1965), whereas the basal lip of Little Coum lies

738   at 262 m asl. In this context, Manley (1961) argued that cirques in the Howgill Fells lack

739   evidence for reoccupation during the Younger Dryas because they are too low. Norris and

740   Evans (2017) suggested the ELA in the western Pennines was 580 m asl during the Younger

741   Dryas with the lowest estimate placing the altitude at 445 m asl (Wilson and Clark, 1995).

742   Similarly, in the eastern Lake District, immediately to the north-west of Great Coum, the ELA

743   has been estimated at 400–600 m with 400 m being regarded as distinctly marginal (Wilson

744   and Clark, 1998). Glacial ice only descended to altitudes below 400 m asl where small outlet

745   glaciers were fed from plateau icefields (McDougall, 2013), the extents of which remain

746   controversial (Bickerdike *et al.*, 2018). In this respect, Harvey (1997) noted that there was

747   no evidence of ice readvance in the west facing Carlingill, neighbouring Great Coum.

748

749   As the top of the headwall of Great Coum is at 468 m asl, with no extensive plateau above, it

750   seems unlikely that snow supply was sufficient to maintain a Younger Dryas cirque glacier.

751   Others have also noted that Howgill cirques are too low to support Younger Dryas ice but

752   have suggested that the 'fresh' appearance of moraines in some Howgill and western

753   Pennine cirques indicate that Younger Dryas ice was maintained locally by extensive snow-

754   blow (Gunson, 1966; Gunson and Mitchell, 1991; Mitchell, 1996). If correct, this would

755   reduce the ELA locally to as low as 311 m asl (Mitchell, 1996). Mitchell's estimate of ELA is

756   similar to the best estimate for Little Coum (300 m asl), and it is noted by several authorities

757   (Manley, 1961; Temple, 1965; Mitchell, 1996) that the dominant wind direction during the

758   Younger Dryas was from the W and SW, associated with cyclonic disturbances.

759   Nevertheless, we are not convinced by this argument. The extensive SW-facing slopes of

760   Grayrigg Forest and Grayrigg Pike are below the Younger Dryas ELA, so it is unlikely that

761   sufficient blown-snow could have been supplied to support glacial ice within the Great and

762   Little Coums. Our exposure age of 18.0 ± 1.2 ka (sample OSF) denoting ice-free conditions

763   on the outer face of the RSF suggests the cessation of glacial erosion at Great Coum.

764

765   **7.0   Conclusions**

766   We have demonstrated that a RSF in the headwall of a cirque in the Lune gorge occurred as

767   a slow downslope movement of an intact rock mass due to the presence of a supporting

768   glacial ice mass buttressing the failed slope. The estimated RSF timing corresponds with

769   regional deglaciation occurring by at least 18.0 ± 1.2 ka.

770

771   Although the case study reported herein supports the role of ice buttressing as a process

772   which may explain arrested RSFs, the vagaries of rock structure from one location to

773   another, coupled with the spatially variable role of isostatic uplift and local meltwater

774   climate (Cave and Ballantyne, 2016) provide strong site-specific controls on the nature and

775   timing of RSFs. Further modelling of RSFs should elucidate the range of conditions

776   associated with incipient failure whilst additional exposure ages for rock surfaces should

777   assist in constraining the timing during which processes such as glacial debuttressing

778   applied.

779

780   **Code availability**

781   *Swedge 6.0* is available from Rocscience Inc., Toronto (www.rocscience.com) for purchase or

782   as a licenced educational package upon application.

783   **Supplement Link**

784   *Note to reviewer: A supplement accompanies this manuscript*

785   **Author Contribution**

786   PAC devised the project and conducted the fieldwork and the *Swedge 6.0* simulations. TS

787   assisted in fieldwork. PAC and JDJ wrote the manuscript. JLA and MFK conducted the

788   cosmogenic nuclide analysis. All authors contributed to the final presentation.

789   **Competing interests**

790   The authors declare that they have no conflict of interest.

791   **Acknowledgements**

798   **Data Availability Statement**

799   The data required as input to *Swedge* version 6.0 (2018) are listed in Table 2. Use of *Swedge*

800   version 6.0 was licensed under an educational agreement with Rocscience Ltd., 2018:

801   www.rocscience.com. The [10]Be concentrations and underlying AMS data associated with the

802   [10]Be exposure ages are published on GitHub

803   https://github.com/CosmoAarhus/LakeDistrict_CosmoData.

804

805   **References**

806   Allen, S. K., Cox, S. C., and Owens, I. F., 2010. Rock avalanches and other landslides in the

807   central Southern Alps of New Zealand: a regional study considering possible climate change

808   impacts. *Landslides*, 8, 33-48.

809

810   Andersen, J.L., Egholm, D.L., Knudsen, M.F., Jansen, J.D., Nielsen, S.B., 2015. The periglacial

811   engine of mountain erosion – Part 1: Rates of frost cracking and frost creep. *Earth Surface*

812   *Dynamics*, 3, 447-462.

813

814   Andersen, J. L., Egholm, D. L., Olsen, J., Larsen, N. K., and Knudsen, M. F. (2020).

815   Topographical evolution and glaciation history of South Greenland constrained by paired

816   26Al/10Be nuclides. *Earth and Planetary Science Letters*, 542, 116300.

817

818   Aveline, W.T., Hughes, T.M., Strahan, A. 1888. The Geology of the Country around Kendal,

819   Sedbergh, Bowness and Tebay. Memoirs of the Geological Survey, England and Wales,

820   London, 94pp plus 3 Plates.

821

822   Ballantyne, C.K. 2002. Paraglacial geomorphology. *Quaternary Science Reviews*, 21, 1935–

823   2017.

824

825   Ballantyne, C.K., Periglacial Geomorphology, Wiley, 472pp, 2018.

826

827   Ballantyne, C. K., Wilson, P., Gheorghiu, D. and Rodés, À., 2014. Enhanced rock-slope failure

828   following ice-sheet deglaciation: timing and causes. *Earth Surface Processes and Landforms*,

829   39, 900–913.

830

831   Barr, I.D., Ely, J.C., Spagnolo, M., Clark, C.D., Evans, I.S., Pellicer, X.M., Pellitero, R., Rea, B.R.

832   2017. Climate patterns during former periods of mountain glaciation in Britain and Ireland:

833   Inferences from the cirque record. *Palaeogeography, Palaeoclimatology, Palaeoecology*,

834   485, 466–475.

835

836   BGS (British Geological Survey), http://www.bgs.ac.uk/data/boreholescans/home.html,

837   accessed 2022, undated.

838

839   BGS, 2008a. Geological Survey of England and Wales 1:50,000 geological map series, New

840   Series Sheet 39, Bedrock, Kendal.

841

842   BGS, 2008b. Geological Survey of England and Wales 1:50,000 geological map series, New

843   Series Sheet 39, Bedrock and Superficial Deposits, Kendal.

844

845   Bickerdike, H.L., Ó Cofaigh, C., Evan, D.J.A., Stokes, C.R., 2018. Glacial landsystems, retreat

846   dynamics and controls on Loch Lomond Stadial (Younger Dryas) glaciation in Britain. *Boreas*,

847   47, 202-224.

848

849   Bonilla-Sierra, V., Scholtès, L., Donzé, F.-V., Elmouttie, M. 2015. DEM analysis of rock bridges

850   and the contribution to rock slope stability in the case of translational sliding failures.

851   *International Journal of Rock Mechanics and Mining Sciences*, 80, 67–78.

852

853   Bovis, M.J. 1982. Uphill-facing (antislope) scarps in the Coast Mountains, southwest British

854   Columbia. *Geological Society of America Bulletin*, 93, 804-812.

855

856   Brown, V.H., Evans, D.J.A., Evans, I.S. 2011. The glacial geomorphology and surficial geology

857   of the south-west English Lake District. *Journal of Maps*, 7, 221–243.

858

859   Brown, V. H., Evans, D. J. A., Vieli, A. and Evans, I. S. 2013. The Younger Dryas in the English

860   Lake District: reconciling geomorphological evidence with numerical model outputs. *Boreas*,

861   42, 1022–1042.

862

863   Carling, P.A., Su, T., Meshkova, L., 2023. Distribution of Devensian glacial erratics and related

864   evidence elucidate complex ice flow changes across a former ice divide: Northern England.

865   *Proceedings of the Geologists' Association*, 134, 139-165.

866

867   Cave, J.A.S. and Ballantyne, C.K., 2016. Catastrophic rock-slope failures in NW Scotland:

868   quantitative analysis and implications, Scottish *Geographical Journal*, 132, 185-209.

869

870   Chiverrell , R.C. and Thomas, G.S.P., 2010. Extent and timing of the last glacial maximum

871   (LGM) in Britain and Ireland: a review. *Journal of Quaternary Science*, 25, 535-549.

872

873   Chiverrell, R.C., Smedley, R.K., Small, D., Ballantyne, C.K., Burke, M.J., Callard, S.L., Clark,

874   C.D., Duller, G.A.T., Evans, D.J.A., Fabel, D., Van Landeghem, K., Livingstone, S.,

875   O Cofaigh, C., Thomas, G.S.P., Roberts, D.H., Saher, M., Scourse, J.D., Wilson, P., 2018.

876   Ice margin oscillations during deglaciation of the northern Irish Sea Basin. *Journal*

877   *of Quaternary Science*, https://doi.org/10.1002/jqs.3057 (ISSN 0267-8179).

878

879   Clark, P.U., Dyke, A.S., Shakun, J.D., Carlson, A.E., Clark, J., Wohlfarth, B., Mitrovica, J.X.,

880   Hostetler, S.W., McCabe, M., 2009. The last glacial maximum. *Science*, 325, 710–714.

881

882   Clark, C.D., Ely, J.C., Greenwood, S.L., Hughes, A.L.C., Meehan, R., Barr, I.D., Bateman, M.D.,
883   Bradwell, T., Doole, J., Evans, D.J.A., Jordan, C.J., Monteys, X., Pellicer, X.M. Sheehy, M.,
884   2018. BRITICE Glacial Map, version 2: a map and GIS database of glacial landforms of the last
885   British–Irish Ice Sheet. *Boreas*, 47, 11–27. https://doi.org/10.1111/bor.12273.
886

887   Cody, E., McColl, S., Draebing, D., Cook, S., 2018. Structural control and development of the

888   ice buttressed Mueller rockslide, New Zealand. Geophysical Research Abstract 30, EGU2018-

889   10748, EGU General Assembly 2018.

890

891   Colgan, W., Arenson, L.U., 2013. Open-pit glacier ice excavation: brief review. *Journal of Cold*

892   *Regions Engineering*, 27, 223-243.

893

894   Cossart E, Braucher R, Fort M, Bourlès DL, Carcaillet J. 2008. Slope instability in relation to

895   glacial debuttressing in alpine areas (Upper Durance catchment, southeastern France):

896   Evidence from field data and 10Be cosmic ray exposure ages. *Geomorphology*, 95: 3–26.

897

898   Davies, B.J., Livingstone, S.J., Roberts, D.H., Evans, D.J.A., Gheorghiu, D.M., Ó Cofaigh, C.,

899   2019. Dynamic ice stream retreat in the central sector of the last British-Irish Ice Sheet.

900   *Quaternary Science Reviews*, 225, 105989.

901

902   Ehlers, J., Gibbard, P.L., Overview. In: *Encyclopedia of Quaternary Science, vol. 2.*, Elias, S.A.

903   (ed.), Elsevier, Amsterdam, 143-150, 2013.

904

905   Evans, I.S., Cirques and moraines of the Helvellyn Range, Cumbria: Grisdale and Ullswater, In:

906   Geomorphology of the Lake District: A Field Guide, edited by J. Boardman, BGRG Spring Field

907   Meeting, 16-18 May 1997, BGRG, pp. 63-87, 1997.

908

909   Goodchild, J.G., 1875. The glacial phenomena of the Eden valley and the western part of the

910   Yorkshire Dales District. *Quarterly Journal of the Geological Society*, 31, 55-99.

911

912   Goodchild, J.G., 1889. An outline of the geological history of the Eden valley or Edenside.

913   *Proceedings of the Geological Association*, 2, 258-284.

914

915   Gruber, S., Hoezle, M. and Haeberli, W., 2004. Permafrost thaw and destabilization of Alpine

916   rockwalls in the hot summer of 2003. *Geophysical Research Letters*, 31, L13504.

917

918   Gruber, S. and Haeberli, W., 2007. Permafrost in steep bedrock slopes and its temperature-

919   related destabilization following climate change. *Journal of Geophysical Research*, 112,

920   F02S18.

921

922   Gunson, A.R., Some aspects of the Lateglacial Period in the Western Pennines area.

923   Unpublished M.A. thesis, University of Lancaster, 134pp, 1966.

924

925   Gunson, A.R., Mitchell, W.A., Combe Scar, In: Western Pennines: Field Guide, W.A. Mitchell

926   (ed.), Quaternary Research Association, London, pp 104- 110, 1991.

927

928   Harkness, R., 1870. On the distribution of Wastdale-Crag blocks, "Shap-granite boulders" in

929   Westmorland. *Quarterly Journal of the Geological Society*, 26, 517-528.

930

931   Harley, J.B., 1975. Chapter 11 The accuracy of Ordnance Survey maps, In: Ordnance Survey

932   Maps a descriptive manual, HMSO, London.

933

934   Hartmeyer, I., Delleske, R., Keuschnig, M., Krautblatter, M., Lang, A., Schrott, L., Otto, J.-C.,

935   2020. Current glacier recession causes significant rockfall increase: The immediate

936   paraglacial response of deglaciating cirque walls. *Earth Surface Dynamics: Discussions*,

937   https://doi.org/10.5194/esurf-2020-8

938

939   Harvey A.M., Fluvial geomorphology of north-west England. In: Gregory K.J. (ed) Fluvial

940   Geomorphology of Great Britain. The Geological Conservation Review Series. Springer,

941   Dordrecht, 173-200, 1997.

942

943   Hasler, A., Gruber, S., Font, M. and Dubois, A., 2011. Advective heat transport in frozen rock

944   clefts: conceptual model, laboratory experiments and numerical simulation. *Permafrost and

945   Periglacial Processes*, 22, 378–389.

946

947   Hilger,P., Hermanns, R.L., Gosse, J.C., Jacobs, B., Etzelmüller, B., Krautblatter, M., 2018.

948   Multiple rock-slope failures from Mannen in Romsdal Valley, western Norway, revealed from

949   Quaternary geological mapping and 10Be exposure dating. *The Holocene*, 28, 1841–1854.

950

951   Hoek, E.T., Bray, J.W., Rock Slope Engineering. 3rd ed. Institute of Mining and Metallurgy,

952   London, 1981.

953

954   Hollingsworth, S.E. 1931. Glaciation of western Edenside and the adjoining areas and the

955   drumlins of Edenside and the Solway plain. *Quarterly Journal of the Geological Society*, 87,

956   281-357.

957

958   Holm, K., Bovis, M., and Jakob, M., 2004. The landslide response of alpine basins to post-

959   Little Ice Age glacial 520 thinning and retreat in southwestern British Columbia,

960   *Geomorphology*, 57, 201-216.

961

962   Hutter, K., Theoretical Glaciology: Material Science of Ice and the Mechanics of Glaciers and

963   Ice Sheets, Springer, 1983.

964

965   Jarman, D., 2005. Large rock slope failures in the Highlands of Scotland: Characterisation,

966   causes and spatial distribution. *Engineering Geology*, 83, 161-182.

967

968   Jarman, D., Wilson, P., Clough Head - Threlkeld Knotts: A perplexing RSF complex. In: The

969   Quaternary of the Lake District - Field Guide, McDougall, D.A. and Evans, D.J.A. (eds)

970   Quaternary Research Association, London, 153–173, 2015a.

971

972   Jarman, D., Wilson, P. 2015b. Anomalous terrain at Dove Crags 'cirqueform' and Gasgale Gill

973   asymmetric valley, English Lake District, attributed to large-scale rock slope failure of pre-

974   LGM origins. *Proceedings of the Yorkshire Geological Society*, 60, 243–257.

975

976   Jaeger, J.C., Cook, N.G.W., Fundamentals of Rock Mechanics, 3rd edn. Chapman and Hall,

977   London, 1979.

978

979   Klimeŝ, J., Novotný, J., Rapre, A.C., Balek, J., Pavel Zahradníĉek, J.C., Strozzi, T., Sana, H., Frey,

980   H., René, M., Štěpánek, P., Meitner, J., Junghardt, J., 2021. Paraglacial rock slope stability

981   under changing environmental conditions, Safuna Lakes, Cordillera Blanca Peru. *Frontiers in*

982   *Earth Science*, 9: 607277. doi: 10.3389/feart.2021.607277

983

984   Lal, D. 1991., Cosmic-ray labeling of erosion surfaces: in situ nuclide production rates and

985   erosion models. *Earth and Planetary Science Letters*, 104, 424-439.

986

987   Le Roux, O., Schwartz, S., Gamond, J.F., Jongmans, D., Bourles, D., Braucher, R., Mahaney,

988   W., Carcaillet, J., Leanni, L., 2009. CRE dating on the head scarp of a major landslide

989   (Séchilienne, French Alps), age constraints on Holocene kinematics. *Earth and Planetary*

990   *Science Letters*, 280: 236–245. https://doi.org/10.1016/j.epsl.2009.01.034

991

992   Letzer, J.M., The glacial geomorphology of the region bounded by Shap Fells, Stainmore and

993   the Howgill Fells in east Cumbria. Unpublished M.Phil. thesis, University of London, 340pp,

994   1978.

995

996   Lifton, N., Sato, T., and Dunai, T. J. (2014). Scaling in situ cosmogenic nuclide production

997   rates using analytical approximations to atmospheric cosmic-ray fluxes. *Earth and Planetary*

998   *Science Letters*, *386*, 149-160.

999

1000   Livingstone, S.J., Evans, D.J.A., Ó Cofaigh, C., 2010. Re-advance of Scottish ice into the Solway

1001   Lowlands (Cumbria, UK) during the Main Late Devensian deglaciation. *Quaternary Science*

1002   *Reviews*, 29, 2544-2570.

1003

1004   Livingstone, S.J., Evans, D.J.A., Cofaigh, C. Ó, Davies, B.J., Merritt, J.W., Huddart, D., Mitchell,

1005   W.A., Roberts, D.H., Yorke, L., 2012. Glaciodynamics of the central sector of the last British-

1006   Irish Ice Sheet in Northern England. *Earth-Science Reviews*, 111, 25–55.

1007

1008   Lowe, J.J., Rasmussen, S.O., Björck, S., Hoek, W.Z., Steffensen, J.P., Walker, M.J.C., Yu, Z.C.

1009   and the INTIMATE group. 2008. Synchronisation of palaeoenvironmental events in the North

1010   Atlantic region during the Last Termination: a revised protocol recommended by the

1011   INTIMATE group. *Quaternary Science Reviews* 27, 6-17.

1012

1013   Manley, G., 1961. The Late-glacial climate of North-West England. *Geological Journal*, 2, 188-

1014   215.

1015

1016   Marr, J.E., Fearnsides, W.G., 1909. The Howgill Fells and their topography. *Quarterly Journal*

1017   *of the Geological Society*, 65, 587- 610 plus plates.

1018

1019   McColl, S.T. 2012. Paraglacial rock-slope stability. *Geomorphology*, 153-154, 1-16.

1020

1021 McColl, S.T., Davies, T.R.H., McSaveney, M.J. 2010. Glacier retreat and rock-slope stability:

1022 debunking debuttressing. Delegate Papers, Geologically Active, 11th Congress of the

1023 International Association for Engineering Geology and the Environment, Auckland, Aotearoa,

1024 5-10 September 2010, Auckland, New Zealand, 467-474.

1025

1026 McColl, S.T., Davies, T.R.H. 2013. Large ice-contact slope movements: glacial buttressing,

1027 deformation and erosion. *Earth Surface Processes and Landforms*, 38, 1102-1115.

1028

1029 McDougall, D., 2013. Glaciation style and the geomorphological record: evidence for

1030 Younger Dryas glaciers in the eastern Lake District, northwest England. *Quaternary Science*

1031 *Reviews*, 73, 48-58.

1032

1033 Merritt, J.W., Hall, A.M., Gordon, J.E., Connell, E.R., 2019. Late Pleistocene sediments,

1034 landforms and events in Scotland: a review of the terrestrial stratigraphic record. *Earth and*

1035 *Environmental Science Transactions of the Royal Society of Edinburgh,* 110, 39–91.

1036

1037 Miller, S.M., Modelling shear strength at low normal stresses for enhanced rock slope

1038 engineering, In: *Proceedings of the 39th Highway Geology Symposium,* Park City, Utah,

1039 August 17-19, pp 346-356, 1988.

1040

1041 Mitchell, W. A., 1996. Significance of snowblow in the generation of Loch Lomond Stadial

1042 (Younger Dryas) glaciers in the western Pennines, northern England. *Journal of Quaternary*

1043 *Science,* 11**,** 233 - 248.

1044

1045 Moore, J. R., Sanders, J. W., Dietrich, W. E., and Glaser, S. D., 2009. Influence of rock mass

1046 strength on the erosion rate of alpine cliffs. *Earth Surface Processes and Landforms,* 34,

1047 1339-1352.

1048

1049 Moseley, F., 1968. Joints and other structures in the Silurian rocks of the southern Shap Fells,

1050 Westmorland. *Geological Journal*, 6, 79-96.

1051

1052   Moseley F., 1972. A tectonic history of N.W. England. *Quarterly Journal of the Geological*

1053   *Society of London*, 128, 561-598.

1054

1055   Moulson, J.R., Some Aspects of the Geomorphology of the Lune Basin. Unpublished M.A.

1056   thesis, University of Manchester, 1966.

1057

1058   Norris, S.L., Evans, D.J.A., High Cup Plain – a Younger Dryas palaeoglacier. In: Evans D.J.A.

1059   (ed.), The Quaternary Landscape History of Teesdale and the North Pennines – Field Guide.

1060   Quaternary Research Association, London, pp. 231-236, 2017.

1061

1062   Porter, S.C. 2001. Snowline depression in the tropics during the Last Glaciation. *Quaternary*

1063   *Science Reviews*, 20, 1067-1091.

1064

1065   Rasmussen, S. O., Andersen, K. K., Svensson, A. M., Steffensen, J. P., Vinther, B. M., Clausen,

1066   H. B., Siggaard-Andersen, M.-L.; Johnsen, S. J., Larsen, L. B.; Dahl-Jensen, D., Bigler, M.,

1067   2006. A new Greenland ice core chronology for the last glacial termination. *Journal of*

1068   *Geophysical Research*, 111 (D6): D06102.

1069

1070   Rocscience Ltd., SWEDGE-Probabilistic analysis of the geometry and stability of surface

1071   wedges. Toronto, Canada; www.rocscience.com, 2018.

1072

1073   Rose, J., Letzer, J.M., 1977. Superimposed drumlins. *Journal of Glaciology*, 18, 471-480.

1074

1075   Rose, J., 1985. The Dimlington Stadial/Dimlington Chronozone: a proposal for naming the

1076   main glacial episode of the Late Devensian in Britain. *Boreas* 14, 225-230.

1077

1078   Sanders, J.W., Cuffey, K.M., Moore, J.R., MacGregor, K.R., Kavanaugh, J.L., 2012. Periglacial

1079   weathering and headwall erosion in cirque glacier bergschrunds. *Geology*, 40, 779-782.

1080

1081   Sass, O., 2005. Spatial patterns of rockfall intensity in the northern Alps. *Zeitschrift für*

1082   *Geomorphologie*, 138, 51-65.

1083

Earth **Surface**
Dynamics
Discussions

1084   Scourse, J.D., Haapaniemi, A.I., Colmenero-Hidalgo, E., Peck, V.L., Hall, I.R., Austin, W.E.N.,

1085   Knutz, P.C. and Zahn, R., 2009. Growth, dynamics and deglaciation of the last British-Irish ice

1086   sheet: the deep-sea ice-rafted detritus record. *Quaternary Science Reviews*, 28, 3066-3084.

1087

1088   Sissons, J.B., 1980. The Loch Lomond Advance in the Lake District, northern England.

1089   *Transactions of the Royal Society of Edinburgh: Earth Sciences*, 71, 13-27.

1090

1091   Soper, N.J., The Windermere Supergroup of 1:25,000 sheets NY50 and NY60. Southern Shap

1092   Fells and Northern Howgill Fells, Cumbria. British Geological Survey Technical Report

1093   WA/99/35. 18pp plus 8 figures, 1999.

1094

1095   Soper, N J., Notes on the Windermere supergroup of the country between Kendal and the

1096   River Lune (1: 25 000-scale sheets SD59 and SD69 west). British Geological Survey Internal

1097   Report, IR/06/081. 15pp, 2006.

1098

1099   Stead, D., Wolter, A., 2015. A critical review of rock slope failure mechanisms: the

1100   importance of structural geology. *Journal of Structural Geology*, 74, 1-23.

1101

1102   Stone, P., Millward, D., Young, B., Merritt, J. W., Clarke, S. M., McCormac, M., Lawrence, D. J.

1103   D., Main Late Devensian glaciation of north-west England, In: British Regional Geology:

1104   Northern England. Fifth edition. British Geological Survey, Keyworth, Nottingham,

1105   http://earthwise.bgs.ac.uk/index.php/British regional geology: Northern England, 2010.

1106

1107   Taylor, B.J., Burgess, I.C., Land, D.H., Mills, D.A.C., Smith, D.B., Warren, P.T., Northern

1108   England: British Regional Geology, Fourth Edition, London, HMSO, 125pp, 1971.

1109

1110   Temple, P.H., 1965. Some aspects of cirque distribution in the west-central Lake District,

1111   northern England. *Geografiska Annaler*, 47A, 185-193.

1112

1113   Whalley, W. B., Douglas, G. R., Jonnson, A., 1983. The magnitude and frequency of large

1114   rockslides in Iceland in the postglacial. *Geografiska Annaler*, 65A, 99–110.

1115

1116   Whittall, J., Eberhardt, E., McDougall, S., 2017. Runout analysis and mobility observations for

1117   large open pit slope failures. *Canadian Geotechnical Journal*, 54, 373-291.

1118

1119   Wilson, P. 2005. Paraglacial rock-slope failures in Wasdale, western Lake District, England:

1120   morphology, styles and significance. *Proceedings of the Geologists' Association*, 116, 349–

1121   361.

1122

1123   Wilson, P., Clark, R. 1995. Landforms associated with a Loch Lomond Stadial glacier at

1124   Cronkley Scar, Teesdale, northern Pennines. *Proceedings of the Yorkshire Geological Society*,

1125   50, 277-283.

1126

1127   Wilson, P., Clark, R., 1998. Characteristics and implications of some Loch Lomond Stadial

1128   moraine ridges and later landforms, eastern Lake District, northern England. *Geological*

1129   *Journal*, 33, 73-87.Wilson, P., Clark, R. and Smith, A. 2004. Rock-slope failures in the Lake

1130   District: A preliminary report. *Proceedings of the Cumberland Geological Society*, 7, 13–36.

1131

1132   Wilson, P., Lord, T., 2014. Towards a robust deglacial chronology for the northwest England

1133   sector of the last British-Irish Ice Sheet, *North West Geography*, 14, 1-11.

1134

1135   Wyrwoll, K-H., 1977. Causes of rock-slope failure in a cold area: Labrador-Ungava. *Geological*

1136   *Society of America Reviews in Engineering Geology*, 3, 59–67.

1137

1138

1139

1140

1141

1142

1143

1144

1145

1146

1147